13th ewtec 2019 Proceedings of the 13th European Wave and Tidal Energy Conference 1-6 Sept 2019, Naples, Italy

Comparative study and test on a Wave Energy Point Absorber under various constrains

Xiaofan Li, Qiuchi Xiong, Chien A. Chen, Boxi Jiang, Shuo Chen, Khai Ngo, Robert Parker and Lei Zuo

Abstract— Power generation and motion response of the floating wave energy converters is of great importance in the research topic of ocean energy harvesting. As a classic design for harvesting the ocean wave energy, the wave energy point absorber is commonly studied theoretically using the idealized 1DOF and 2DOF dynamic model based on the number of the free body within the system. Whereas the mooring system is usually ignored and only the heave motion is considered. In this paper, a point absorber is designed prototyped and tested in a water tank under three different constrains, the single body 1DOF, the two body 2DOF and the two body 6DOF. All the designs and configurations are presented in detail. Numerical analysis is conducted and presented as well to help understand the test results deeper. The test results indicate that the two body system can be tuned to match with the wave excitation and achieve higher energy absorption. In addition, the compared results between the 2DOF configuration and 6DOF configuration show that the classic 2DOF dynamic model is able to predict the performance of the point absorber with mooring well.

***Keywords*—Water tank test, Wave Energy Converter**

I. INTRODUCTION

THE study of the wave energy converters (WECs) started at the year of 1799 when the first patent was invented, and attracted much attention from the researchers globally since the world energy crisis happened in the 1970s and 2000s. The overall assessment of the wave energy potential is about 3.7TW globally [1], which is able to cover a large portion of the world energy consumption [2]. In addition, extracting the ocean wave energy not only can relief the tension of increasing world energy demand, it can also benefit the environment as a clean renewable energy [3]. Different concepts and design of WECs have been raised and developed up to date. Among them, point absorber, which adopts the heave oscillation of the free surface of the wave to collect energy, is one of the most widely adopted concepts for harvesting ocean wave energy. In 1975, Budal and Falnes raised the concept of harvest ocean wave energy through a point absorber [4]. The idea soon brought to interest many researchers and much profound theoretical work for feasibility and optimization was done. In 1976, Evans [5] and Mei [6] calculated the maximum power absorption for the single body point absorber, the results show that it can only be achieved through the resonant approach, which is to match the natural frequency of the buoy with the wave frequency. In real applications, however, the frequency of ocean wave can be low to the level of 0.1Hz, leading to an extremely large physical structure of the point absorber which counted as uneconomic and non-feasible [7]. A variety of ideas were raised to overcome this situation. French and Bracewell designed an internal mass to move against the heaving point absorber, springs with different stiffness are adopted to achieve phase control and increase the total energy extraction [8]. Budal et al proposed the latching strategy to reinforce the point absorber to move in phase with the ocean wave for better energy absorption. Bjarte-Larsson and Falnes [9], Babarit et al [10] and Falcao [11] all proposed different strategies, however, their mean idea share the similarity which is to achieve physical resonant through phase control and matching.

Besides the phase control method for a single body point absorber, another widely adopted concept is to connect the floating buoy on the free surface with another submerged body to create a two body structure. For the two body point absorber, the energy is extracted from the relative motion between the two bodies, and no additional mounting frame is needed. In addition, the natural frequency of the system can be tuned through various methods. Falnes derived that for an axisymmetric two

The ID number of this paper submission is 1534. Conference track: Wave device development and testing.

The project is funded by the United States National Science Foundation (NSF) and the United States Department of Energy (DOE).

X. Li, Q. Xiong, B. Jiang and S. Chen now work as research assistant at the Mechanical Engineering Department of Virginia Tech, Virginia, the United States.

C.A. Chen now works as research assistant at the Bradley Department of Electrical and Computer Engineering at Virginia Tech, Virginia, the United States.

Dr. K. Ngo now works as a professor at the Bradley Department of Electrical and Computer Engineering at Virginia Tech, Virginia, the United States.

Dr. R. Parker now works as a professor at the Mechanical Engineering Department of Virginia Tech, Virginia, the United States.

Dr. L. Zuo is the corresponding author of this paper, he now works as a professor at the Mechanical Engineering Department of Virginia Tech, Virginia, the United States. His email address is: leizuo@vt.edu.

body system utilizing heave motion, maximum power absorption can be achieved and the equivalent excitation force can exceed the excitation force on either body [12]. Beatty et al researched into the submerged body and found that with the capability of altering the natural frequency of the submerged body, significant energy absorption increase can be achieved [13]. Korde looked into the arrangement of the two body system and found that the submerged second body could perform better [14]. Liang and Lei explored the effect of mass ratio between the two body and found the optimum and suboptimum condition for both regular and irregular waves [15]. Cândido and Justino [16], Yu and Li [17] and Shami et al [18] also contributed to the two body point absorber on different aspects.

For theoretical studies, the two body self-react point absorber are commonly modelled ideally as a 2 Degree of Freedom (DOF) system where only heave motion is considered. In real applications, however, the prototypes are usually constraint by mooring lines and work in 6DOF where the surge, sway, pitch, row and yaw motion all have influence on the performance [19-21]. In this paper, a wave energy point absorber is designed, analyzed and tested with three different constrains. Firstly, the prototype is works as a single body point absorber and only the heave motion of the floating buoy is considered. Then another submerged body is added to the prototype, both bodies were constraint to be able to move in heave only to mimic the ideal condition. At last, a mooring constrain is added to the two body system and both bodies are able to move in all 6DOF. The results show that the two body design could achieve the effect of frequency tuning and achieve better energy harvesting performance. In addition, the 6DOF motion could influence the performance of the WEC, indicating that the mooring should not be neglected and need to be considered as an important part of the design.

II. DESIGN AND ANALYSIS OF THE WEC

A. *Deployment method*

The typical design for a single body point absorber is illustrated in Figure.1 where a floating buoy moves along the incident wave. The buoy is guided by a rigid structure where in the figure represented by a column. The buoy moves along the structure and is constrained to the heave only direction, thus only one degree of freedom (DOF) z_1 need to be taken into consideration. The motion of the buoy is then adopted to drive the power take-off (PTO) and generate electricity.

As illustrated in Figure.2, the two body wave energy point absorber consist of one floating buoy and a neutrally buoyed submerged body. Energy is absorbed through the relative motion between the two bodies. Such design has the advantage that the natural frequency of the system has high flexibility for adjustment. The study of the two body point absorber usually regard the system as a two body system and only 2 DOF, z_1 and z_2, is considered. For the idealized case in the figure, the column is constrained in all rotary, surge and sway motion to simplify the dynamic analysis.

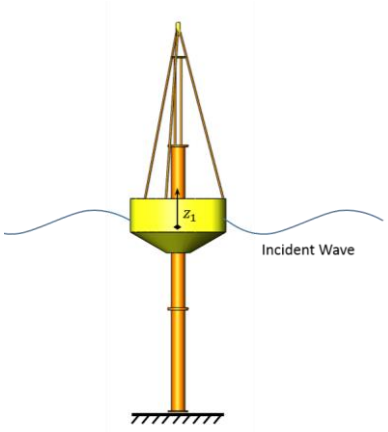

Fig. 1. Prototype deployment for the 1DOF test.

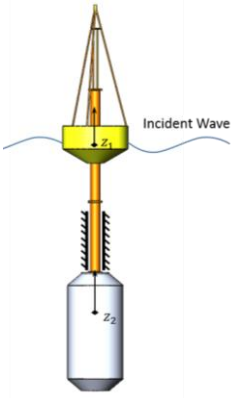

Fig. 2. Prototype deployment for the 2DOF test.

Figure.3 shows the general situation where mooring is added to the two body point absorber. The energy abstraction remain come from the relative motion between the z_1 and z_2. The individual body is free to move in all DOF and the mooring lines will provide soft constrain to the system. The x_1, y_1, z_1, $\emptyset_1$, θ_1 and φ_1 each represents the surge, sway, heave, pitch, row and yaw motion of the floating body. Similarly, the x_2, y_2, z_2, $\emptyset_2$, θ_2 and φ_2 each represents motion of the submerged body respectively.

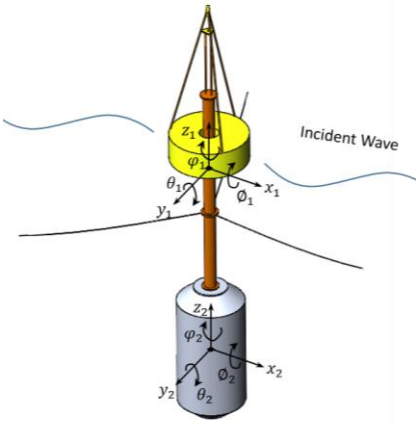

Fig. 3. Prototype deployment for the 6DOF test.

B. PTO dynamic analysis

Different from the common PTO that use a linear damper or a hydraulic system, the proposed prototype use a novel mechanical PTO that use the mechanical motion rectifier (MMR) mechanism to improve the working efficiency and better energy capture capability.

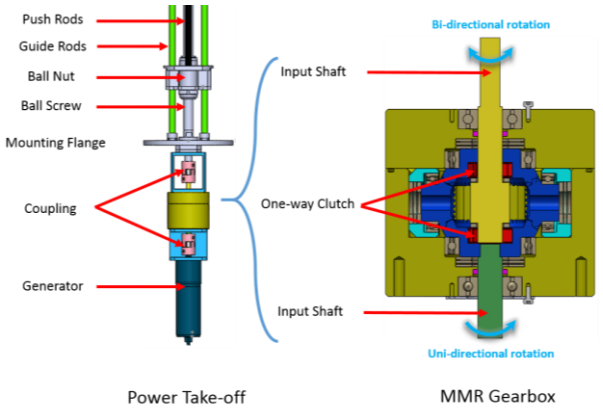

Fig. 4. Design of the MMR PTO.

Figure.4 shows the design of the MMR PTO, The push rods at the top of the PTO is to connect the relative linear motion. In the single body design the motion is the heave motion of the floating buoy, and in the two body system, however, it is the motion between the two bodies. The motion of the push rods is then directed to drive the ball screw. The ball screw is used as a motion converter, where it converts the linear reciprocate motion into bi-directional rotation, two guide rods are assembled in the PTO to counter the torque generated during that process. Through some couplings, the bi-directional rotation is lead to the MMR gearbox where the motion is rectified.

The MMR gearbox illustrated in the right of Figure.4, it consists of one input shaft, one output shaft, three bevel gears, and two one-way clutches which only allow one-directional rotation and lock on the contrary direction. The one-way clutches are inserted between the bevel gears and the input shaft as illustrated. When the input rotation motion is in the clockwise direction, the top one-way clutch disengages and the bottom one engages. The input motion is directly transferred to the output shaft. When the input motion is in the counter-clockwise direction, however, the top one-way clutch engages and the bottom one disengages. The three bevel gears change the direction of the motion to the output is still in clockwise directional rotation. Through this mechanism, the motion of the input is rectified and the output shaft always rotates in one direction. The uni-directional rotation is then finally used for driving the flywheel and the generator. For the non-MMR PTO, the reciprocate rotation from the ball screw is directly lead to the other components below, so the generator always rotates bi-directionally in the speed proportional to the linear motion between the two bodies .

In addition to the motion converting effect, the MMR PTO also possess one unique phenomenon that worthy of further exploration. The effect of the one-way clutch is to lock the rotation between two components in the predetermined direction. The locked rotation, however, is the relative motion between the two components rather than the absolute rotation. When the PTO is driven by the linear motion of the two body WEC, some potential energy is stored in the inertia of the couplings and the generator. When the driving speed decelerates, if the inertia is large enough to keep the generator speed decelerates slower than the driving speed, the stored potential energy starts to be the power source for the generator. Meanwhile, the generator speed is larger than that of the input speed, and both one-way clutches are disengaged. Then the PTO is decoupled into two subsystems, one is the MMR gearbox driven by the ball screw without load, and the other is the self-powering subsystem where the inertia stored energy powers the generator. This unique phenomenon can be expressed more explicitly through numerical simulation [22].

When the input shaft speed is larger than or equal to the speed of the output shaft, the motion from the ball nut will drive the ball screw to rotate in the speed of:

$$\omega_{bs} = \frac{2\pi \dot{z}}{l_b}$$

where, ω_{bs} is the rotation speed of the ball screw, $\dot{z}$ is the linear relative speed input toward the PTO, l_b is the lead distance of the ball screw. With a gearhead on the geared generator, the rotation speed of the generator will increase at the ratio of the gearhead, $\omega_{ge} = n_g \omega_{bs}$, whereas ω_{ge} is the rotation speed of the generator and n_g is the gear ratio.

For the DC generator used in the prototype, the torque of the generator T_{ge} is proportional to two parameters of the generator, one is K_e, which is the electric constant between the output voltage and the rotation speed of the generator; the other one is K_t, which is the torque constant between the electric current and the reactive torque on the generator [23]:

$$T_{ge} = \frac{K_t K_e \omega_{ge}}{(R_{in} + R_{ex})}$$

Here R_{in} and R_{ex} are the inner and outer resistive load of the generator.

Combining the relationships of these mechanical components together, the damping coefficient c_{e_en} between the generator and the linear motion input for the system when it engages could be presented as:

$$c_{\mathrm{e\_en}} = \frac{K_t K_e}{(R_{in} + R_{ex})} \frac{4\pi^2}{{l_b}^2} {n_g}^2$$

Using the Lagrange Equation, the dynamic equation for the overall PTO system when it is engaged can be written as:

$$m_{pto}\ddot{z} = f_{pto} - c_{\mathrm{e\_en}}\dot{z}$$

Where, f_{pto} is the force cast on the PTO system, m_{pto} is the equivalent mass of the PTO.

However, when the system disengages, the total system decouples into two separate subsystems, by using the similar approach, the equation can be acquired that for the electric damping of the disengaged system:

$$c_{e\_dis} = \frac{K_t K_e}{(R_{in} + R_{ex})} {n_g}^2$$

Since the mass from the push rod and ball nut are small and is able to be neglected, the equation for the two decoupled system is:

$$\begin{cases} 0 = f_{pto} \\ m_e \dot{\omega_{ge}} + c_{e\_dis}\omega_{ge} = 0 \end{cases}$$

Here, m_e is the equivalent mass provided by the inertia of gearbox and generator. By solving the equation above, it can be found out that the solution for the rotation speed of ω_{ge} is:

$$\omega_{ge} = e^{kt}$$

Here,

$$k = \frac{-c_{e\_dis}}{m_e}$$

This result shows that after the disengagement happens, the rotation speed of the generator will die out exponentially, and two factors can influence the speed of that, one is the total equivalent mass of the system and the other is the electric damping of the system.

C. *Analysis of different constrains*

Since the single body point absorber is constrained to heave motion, only one degree of freedom (DOF) need to be considered, the motion is labelled as z_1 in the figure. Hence the equation of motion for the single body point absorber can be obtained as:

$$m_1 \ddot{z}_1 = f_{e1} + f_{pto} + f_{hs1} + f_{r1} + f_{v1}$$

Here,

m_1 is the mass of the floating buoy

$\ddot{z}_1$ is the acceleration of the buoy in heave motion

f_{e1} is the excitation force cast on the buoy from the wave

f_{pto} is the force from the PTO system

f_{hs1} is the hydrostatic restoring force

f_{r1} is the radiation force from the body-wave interaction

f_{v1} is the viscous force

Explicitly, the excitation force f_{e1} is a frequency dependent term that can be calculated through the boundary element method (BEM). The radiation force f_{r1} is consist of two terms, one is from the radiation damping and the other is from the added mass, these two terms are also frequency dependent terms that can be acquired through BEM, and the radiation force can be introduced using Cummins equation [24]:

$$f_{r1} = -A(\infty)\ddot{z}_1 - \int_0^t k(t-\tau)\dot{z}_1(\tau)d\tau$$

$$k(t) = \frac{2}{\pi}\int_0^\infty b(\omega)cos\omega t\, d\omega$$

A(∞) is the added mass obtained with linear wave theory when the frequency approaches to infinity, $b_{ij}(\omega)$ is the frequency dependent radiation damping, in this specific case, these parameters are acquired through WAMIT [25].

Besides the excitation force and radiation force, the f_{hs1} is the hydrostatic restoring force which is proportional to the section area of floating buoy on the surface of the wave, f_{v1} is the additional viscous force from the viscous damping terms, and f_{pto} is the force from the PTO, based on the previous introduction, the PTO force for the single body system can be introduced as:

$$f_{pto} = \begin{cases} -m_e\ddot{z}_1 - c_{\mathrm{e\_en}}\dot{z}_1 & Engage \\ 0 & Disengage \end{cases}$$

Similarly, for the two body wave energy point absorber, where the floating buoy and submerged body interact with each other, the dynamic analysis need to be taken into the consideration of the individual body and can be described as:

$$m_1\ddot{z}_1 = f_{e1} + f_{pto} + f_{hs1} + f_{r1} + f_{v1}$$
$$m_2\ddot{z}_2 = f_{e2} - f_{pto} + f_{hs2} + f_{r2} + f_{v2}$$

The parameters listed in the second equation has the same physical meaning with the equation listed for the single body design. The radiation force on the two different bodies can be presented as:

$$f_{r1} = -A_{11}(\infty)\ddot{x}_1 - A_{12}(\infty)\ddot{x}_2 - \int_{-\infty}^{t} k_{11}(t-\tau)\dot{x}_1(\tau)d\tau - \int_{-\infty}^{t} k_{12}(t-\tau)\dot{x}_2(\tau)d\tau$$

$$f_{r2} = -A_{22}(\infty)\ddot{x}_2 - A_{21}(\infty)\ddot{x}_1 - \int_{-\infty}^{t} k_{21}(t-\tau)\dot{x}_1(\tau)d\tau - \int_{-\infty}^{t} k_{22}(t-\tau)\dot{x}_2(\tau)d\tau$$

$$k_{ij}(t) = \frac{2}{\pi}\int_0^\infty b_{ij}(\omega)cos\omega t\, d\omega \ (i,j = 1,2)$$

Here,

$A_{11}(\infty)$ and $A_{22}(\infty)$ are the added mass obtained from either body itself when the frequency approaches to infinity

$A_{12}(\infty)$ and $A_{21}(\infty)$ are the added mass obtained from interaction between the two bodies when frequency approaches to infinity

$b_{11}(\omega)$ and $b_{22}(\omega)$ are the frequency dependent radiation damping obtained from the either body itself

$b_{12}(\omega)$ and $b_{21}(\omega)$ are the frequency dependent radiation damping obtained from interaction between the two bodies

In the two body design, the energy is absorbed from the relative motion between the two bodies, thus the PTO force f_{pto} is modified to:

$$f_{pto} = \begin{cases} -m_e(\ddot{z}_1 - \ddot{z}_2) - c_{e\_en}(\dot{z}_1 - \dot{z}_2) & Engage \\ 0 & Disengage \end{cases}$$

As for the 6DOF test, where all the motions need to be considered, the equation of motion for the individual body can be presented as

$$\boldsymbol{M_1\ddot{X}_1} = \boldsymbol{F_{e1}} + \boldsymbol{F_{pto}} + \boldsymbol{F_{hs1}} + \boldsymbol{F_{r1}} + \boldsymbol{F_{v1}} + \boldsymbol{F_{m1}}$$
$$\boldsymbol{M_2\ddot{X}_2} = \boldsymbol{F_{e2}} - \boldsymbol{F_{pto}} + \boldsymbol{F_{hs2}} + \boldsymbol{F_{r2}} + \boldsymbol{F_{v2}} + \boldsymbol{F_{m2}}$$

Here, $\boldsymbol{M_1}$ and $\boldsymbol{M_2}$ are the 6×6 mass matrix containing the mass and moment of inertia of the individual body. $\boldsymbol{\ddot{X}_1}$ and $\boldsymbol{\ddot{X}_2}$ are the 6×1 acceleration matrix on each degree of freedom. The other force are all 6×1 matrix for the previously introduced force on all 6DOF. $\boldsymbol{F_{m1}}$ and $\boldsymbol{F_{m2}}$ are the mooring force applied on the body. As the energy harvested from the prototype remain obtained from the relative motion in heave between the two bodies, the PTO

force $\boldsymbol{F_{pto}}$ can be presented as following, whereas f_{pto} is the PTO force obtained from the 2DOF equation,

$$\boldsymbol{F_{pto}} = \begin{bmatrix} 0 \\ 0 \\ f_{pto} \\ 0 \\ 0 \\ 0 \end{bmatrix}$$

Mooring structure introduced in the paper is the illustrated in Figure.3. Three mooring lines are fixed on the mooring plate on the submerged body and provide recovering force and constrain the WEC at an ideal position. As the mooring lines are simply fixed lines with soft spring, the mooring line dynamics is neglected in this paper and the mooring force is substituted by a matrix of mooring stiffness and mooring damping coefficient.

This simulation presented in this paper is conducted using the WEC-Sim, an open-source WEC simulation tool [26]. The mooring configuration is simulated using the features of mooring matrix as the mooring setup in this paper is simple.

III. PRELIMINARY TEST AND SETUP

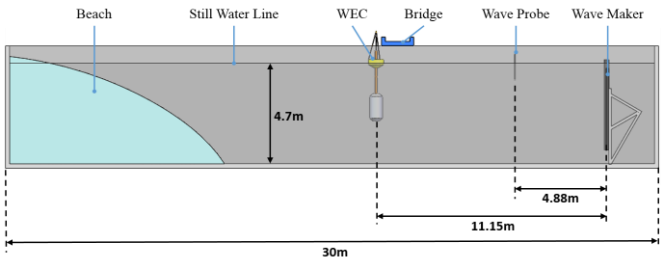

Fig. 5. Configuration of the water tank used for testing.

To further verify the performance of the proposed WEC, the prototype was then assembled and tested in the water tank from the Alfond W2 Ocean Engineering Lab in the University of Maine. The general test configuration is illustrated in Figure.5. The water tank is 30 meters in length, 9 meters in width and the water depth is 4.7 meters. The beach of the water tank has a porous structure, which is able to absorb the incident wave hit on the beach and minimize the influence the reflection wave to the WEC. A wave probe was set at 4.88 meters away from the wave maker to monitor the wave condition during the test and give feedback to the wave generator. The WEC prototype was placed 11.15 meters from the wave maker, where a bridge with high structure stiffness is adopted as mounting platform for different types of constrains.

Fig. 6. Mass property identification test.

In order to characterize the WEC dynamic precisely and verify the previous simulation results, body mass property test and free decay tests were conducted separately for both bodies to identifying the unknown terms. Figure.6 describe the body identification for the buoy and the second body, they were lifted by a forklift and swung in air to acquire the property of center of the gravity and the dry mass, same approach is used for the buoy as well. Other properties including the moment of inertia in different directions are obtained through the test as well. The foam added in the figure is to increase the buoyance of the designed submerged body so it can achieve the status of neutrally buoyed at the desired position of the free surface.

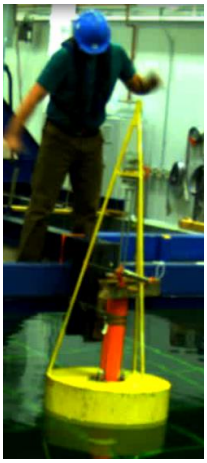

Fig. 7. Free decay test of the floating buoy.

Figure.7 shows the free decay test of the floating buoy. In the free decay test for the buoy, floating buoy was pushed into water with an initial displacement first. Due to the hydrostatic restoring force, the body started to move in heave when it was released. And the motion gradually decayed as the result of radiation damping and drag damping. Similar approach was used for the second body as well.

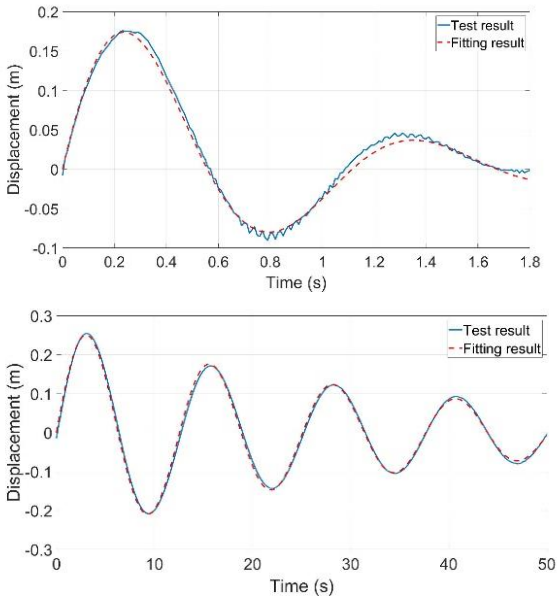

Fig. 8. Top: Free decay test result and the fitting result of the floating buoy. Bottom: Free decay test result and the fitting result of the submerged body.

Figure.8 shows the free decay test results for the two bodies. The result was then used through curve fitting to verify the hydro parameters. The added mass parameters matches well with the simulation results, the damping terms, however, is larger. This is due to the drag damping, as the result, additional viscous damping coefficient is added based on the curve fitting results as compensation.

Through the preliminary test of the mass property and free decay. The unknown and unverified physical parameters of the prototype is obtained. These parameters is put into the dynamic model of the prototype, thus the model is refined and can achieve better simulation accuracy.

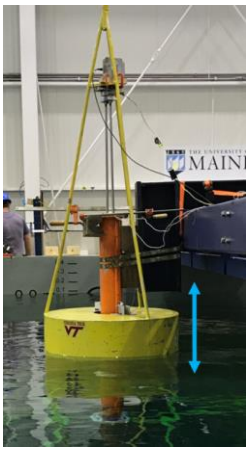

Fig. 9. 1DOF test setup, the blue arrow indicates the motion of the floating buoy.

To compare the power generation of three different types of constrains, the water tank test of the proposed prototype is set up in three different ways. Figure.9 illustrates the setup of 1DOF prototype where the column is fixed on the bridge through clamps and only the floating buoy is able to move in heave.

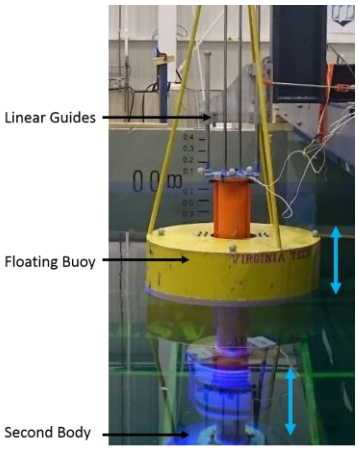

Fig. 10. 2DOF test setup, the blue arrows indicate the motion of either body.

Figure.10 shows the setup of the 2DOF test, a linear guide system is used for the second body as illustrated in the figure. Both the floating buoy and the second body is restricted to the heave motion only.

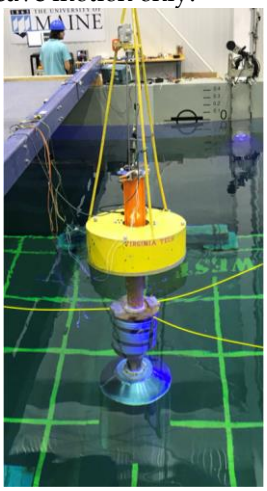

Fig. 11. 6DOF test setup, the yellow lines denotes the directions of the mooring line.

Figure.11 shows the test setup for the 6DOF system, three mooring lines are fixed on the proposed prototype to provide the mooring force as illustrated.

To acquire necessary data from the tests. A load cell was assembled between the floating buoy and the submerged body to record the force input towards the PTO. The relative motion between the two bodies was monitored by a string pot, and the output voltages from the generator at different electrical resistances were recorded as well. In addition, a Qualisys motion capture system [27] was used to measure the motion of each body. All the signals from the sensors were loaded into a DAQ system, a fourth order Butterworth numerical filter as shown in Figure.12 is adopted to eliminate the noise.

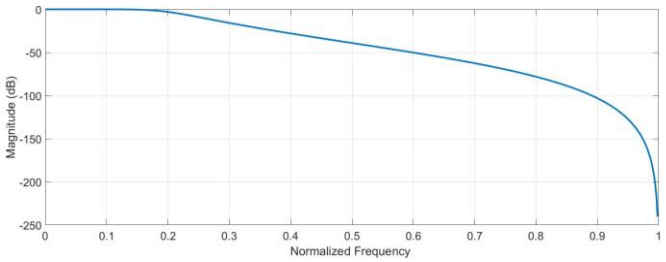

Fig. 12. Property of the 4th order Butterworth filter used in the test.

Table I lists the regular and irregular wave conditions used during the test, which were adapted from the DOE Wave Energy Prize's tests [28] for 1:30 scale model using Froude scaling [29]. In addition to the wave probe used during the testing, two more wave probes were used to calibrate the wave before the test to guarantee the wave accuracy. Test for each wave condition was conducted three times to verify the consistency. Each single test last for 5 minutes to spare enough time for the WEC to reach steady state.

TABLE I
WATER TANK TEST WAVE PARAMETERS

Regular Wave No.	Wave Period (s)	Wave Length (m)	Wave Height (m)	Power Flux (W/m)
1	1.24	4.22	0.053	4.37
2	1.83	5.20	0.065	7.40
3	2.01	6.30	0.079	11.91
4	2.19	7.49	0.094	18.41
5	2.37	8.80	0.110	27.46
6	2.56	10.20	0.128	39.78
7	2.74	11.71	0.146	56.17
Irregular Wave	Dominant Wave Period (s)		Significant Wave Height (m)	
1	2.83		0.173	

IV. RESULTS AND DISCUSSION

As the power absorbed by the prototype from the incident wave is not all transferred into usable electricity, two criteria are used in this paper to evaluate the performance of the proposed prototype. One is the transient mechanical input power P_{in} which represents the total energy input towards the PTO and it can be presented as:

$$P_{in} = f_{pto}\dot{z}_{pto}$$

Here, f_{pto} is read from the load cell and $\dot{z}_{pto}$ is obtained through the derivation of the displacement acquired from the string pot.

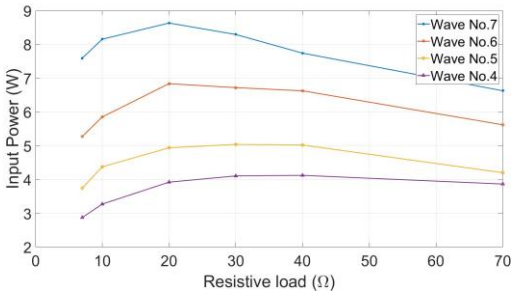

Fig. 13. Input power of the 1DOF test under regular wave with different resistive load.

In addition to the input power, the other measurement is the transient usable electric power P_{out} acquired from the incident wave, which can be described as:

$$P_{out} = \frac{V_{out}^2}{R_{ex}}$$

Here, R_{ex} is the resistance of the external electric power resistor used during the test, V_{out} is the output voltage on the external resistor. The averaged input and output power can be calculated through the time averaging method on the integral of the transient power.

Due to the small wave elevation and reactive motion, the test results for the regular wave No.1, 2 and 3 will not be discussed here. Figure.13 shows the test results of the input power for the 1DOF setup with different resistive load. A series of outer resistor with different resistance was chosen in order to find the optimum. As the resistive load goes higher, the electric damping coefficient goes smaller. The optimum damping coefficient is able to be observed through the figure, for wave No.7 the optimum resistive load is about 20Ω and it shift to about 40Ω at wave No.4. This shifting phenomenon is resulted from the change of the excitation frequency of the wave, and can be derived analytically [30]. In brief, the optimum condition for energy absorption happens when the damped frequency of the system match with the excitation frequency, as the excitation frequency changes, the optimum damping coefficient change as well.

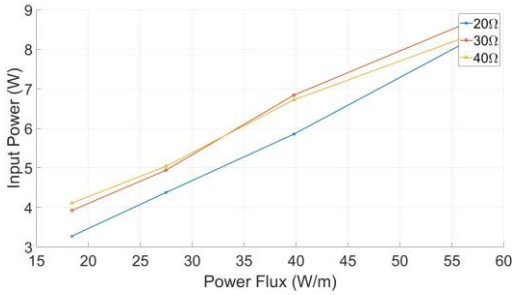

Fig. 14. Input power of the 1DOF test under regular wave with different power flux.

Figure.14 shows the same result with Figure.13 using a different scale. The input power to the system around the optimum resistive load is shown in the figure. The power flux is read from Table I. It is observed that the input power is close to a linear relationship with the power flux, which represents the capture width ratio is also close to linear. This result indicate that the optimum wave excitation frequency does not exist for the 1DOF test, and the system does not resonant.

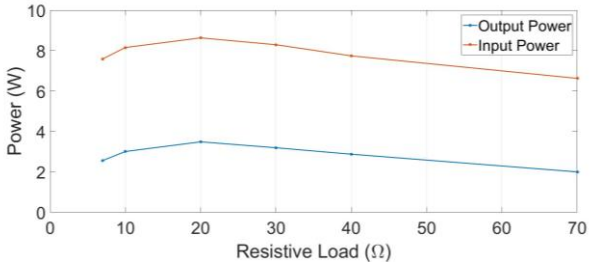

Fig. 15. Compare between the input power and output power of the 1DOF test under regular wave.

The compare between the input mechanical power and the output electrical power under the wave No.7 is shown in Figure.15. The efficiency of the system can be acquired by dividing the illustrated parameters. The energy dissipation between the input power and output power mainly from two parts, one is the mechanical loss due to friction and collision of the mechanical components, the other is the electric loss from the inner resistance of the

generator. The electric loss can be improved by using a larger external resistor to reduce the portion of the energy consumption of the inner resistance. This also indicate that the electric damping is only one part of the overall damping, a reasonable result can only be acquired with a better characterization of the PTO to include the mechanical damping as well, thus the overall optimum condition for the system can be found.

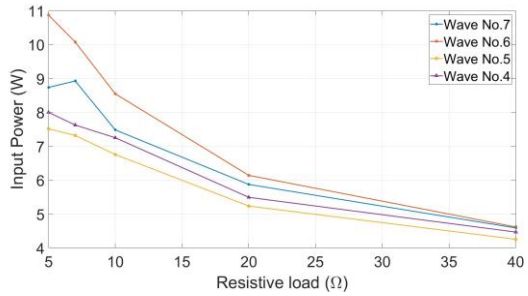

Fig. 16. Input power of the 2DOF test under regular wave with different resistive load.

Figure.16 shows the input power of the 2DOF test with different resistive load. As illustrated in the figure, the optimum point didn't show up even when a very small external resistor is used. This indicate that the optimum damping coefficient for the 2DOF system is relatively large and better results should be obtained. One possible way of solving this problem is to choose a generator with greater rated power at the same condition. However, the maximum power absorption of the 2DOF system was not achieved during the proposed test.

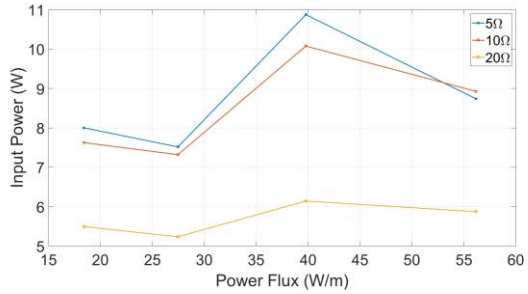

Fig. 17. Input power of the 2DOF test under regular wave with different power flux.

The other scale of the previous 2DOF result is presented in Figure.17. The maximum power absorption acquired from the test is with wave No.6 which has a smaller power flux. This results verified that compared with the 1DOF single body structure, the two body system has a better tuning flexibility to match with the wave frequency [15].

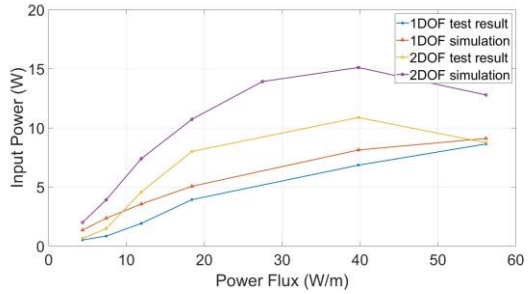

Fig. 18. Compare between the simulation and test results for 1DOF and 2DOF test under regular wave.

Figure.18 compares the input power for the 1DOF and 2DOF system, both test results and simulation results are illustrated in the figure. The results show that the two body system has a better performance even when the optimum damping coefficient was not achieved during the test. The simulation results for the single body design match well with the test results. For the two body system, the simulation trend match well with trend of the test result, however, the performance of the system can be further improved. In addition, the friction of the mechanical system is modeled as a Coulomb damping in the WEC-Sim and the value of the damping may not be the true friction applied to the system when testing, this may also lead to the energy acquired from the simulation results to be higher.

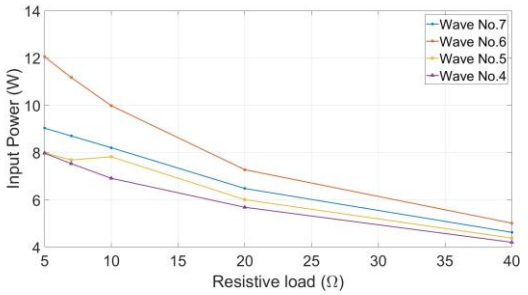

Fig. 19. Input power of the 6DOF test under regular wave with different resistive load.

Another topic this paper would like to discuss is the feasibility of using the 2DOF model to simulate the 6DOF system in the real applications with mooring implemented. Figure.19 shows the input power of the 6DOF test results. The results shows good coherence with the results in Figure.16 and the input power is close to the 2DOF setup, which preliminarily proves the hypothesis that the 2DOF model can be used for predicting the performance of the WEC in real application with mooring.

According to the linear wave theory, a drift force f_d will cast on the WEC as it absorbs energy from the propagating wave. This force need to be counter balanced by the mooring lines and the minimum of the force can be introduced as [30]:

$$f_{d.min} = \frac{\omega}{g} P_{in}$$

Here, the ω is the angular velocity of the wave and g is the acceleration of gravity. For the proposed prototype and wave condition, this force is as small as several Newton, this is used as the criteria for choosing a property spring stiffness for the mooring lines.

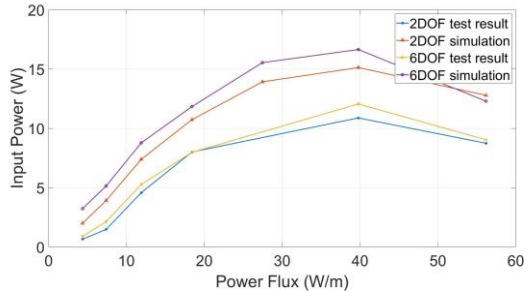

Fig. 20. Compare between the simulation and test results for 2DOF and 6DOF test under regular wave.

Figure.20 compares the test results and simulation results for the 2DOF and 6DOF setup under the excitation of the wave No.7. The simulation results show that under the same condition, the 6DOF setup should possess better energy generation. The test results proved the simulation results as the input power for the 6DOF is larger. Figure.21 shows the time domain test results for the relative motion between the two bodies under the excitation of wave No.7 with 5Ω external resistance. It can be observed that due to the free motion in all degrees of freedom, the 6DOF has a larger relative motion which lead to higher total input power.

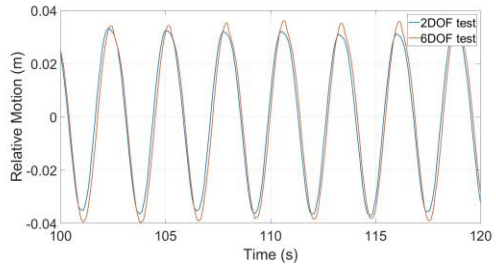

Fig. 21. Time domain test result of 2DOF and 6DOF test under wave No.7 with 5Ω external resistance.

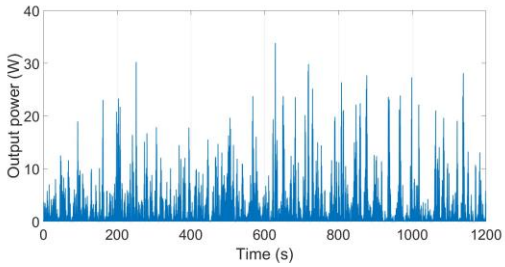

Fig. 22. Output power of the 1DOF irregular wave test.

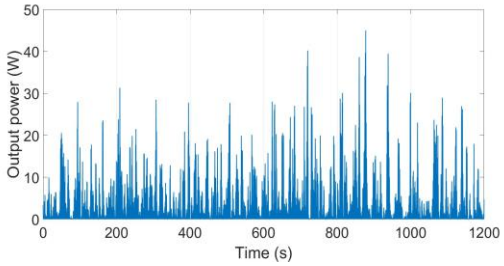

Fig. 23. Output power of the 2DOF irregular wave test.

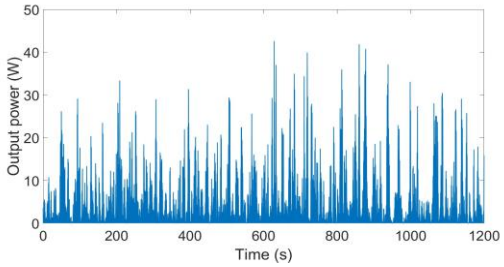

Fig. 24. Output power of the 6DOF irregular wave test.

In addition to the regular wave test, the irregular wave test was conducted to verify the performance of different setups. Figure.22 to Figure.24 show the time domain output power of three different setups. For the 1DOF test, the peak power acquired from the test is 33.82W and the average power is 2.04W, the 2DOF test has a peak power of 44.98W and an average power of 2.61W whereas the 6DOF has a peak power of 43.90W and an average power of 2.44W. It worth to be pointed out that although the 2DOF test has a larger output power over the 6DOF test, the input mechanical power of the 6DOF test remains greater. This is because the pitch, row and yaw motion will increase the pressure onto the PTO and lead to a larger friction, thus the mechanical energy loss become greater and lead to a low energy transfer efficiency. The overall energy transfer efficiency between input power and output power is 38.89%, 40.70% and 33.93 for the 1DOF, 2DOF and 6DOF test.

It is easy to observe that the 2DOF and 6DOF irregular wave test results shares same trend for the power generation. For better observation, Figure.25 illustrates the time domain relative motion result of the irregular wave test in a zoomed one minute section. The result shows that the motion of the 2DOF and 6DOF test match with each other well, indicating that with a reasonably designed mooring system, using the simplified 2DOF model could still predict the performance of the WEC with an acceptable error rate.

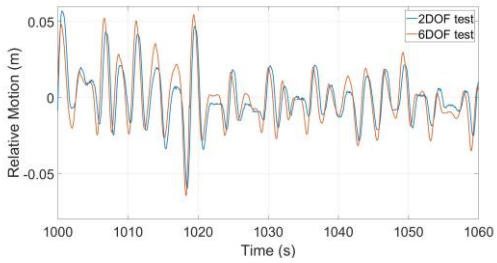

Fig. 25. Result of the relative motion for the 2DOF and 6DOF test in zoomed section.

V. CONCLUSION AND FUTURE WORK

In this paper, a wave energy point absorber is designed, prototyped, simulated and tested under three different constrains. The test results with different test conditions and constrains are presented to verify two objectives. One is that compared with the single body 1DOF point absorber, the two body 2DOF system has a better energy capture potential, and can be adjusted to resonant with the wave excitation frequency for optimum power absorption. The second objective this paper has verified is that for a two body point absorber working in real conditions with mooring and is able to move in all 6DOF. If the mooring system is designed reasonably not to over constrain the motion of the WEC, the performance of the WEC can be predicted with an acceptable error using a simplified 2DOF dynamic model.

The future work for this paper consist of three parts, the first one is to build more detailed model for the 6DOF set up, a refined dynamic model for the mooring system is able to improve the accuracy of the simulation. In addition, a refined model with better precision for the PTO is required as the current friction model is not capable of matching with the test results well. Last but not least, the test results obtained from the test is able to be used to guide the future design of the WEC, further improvement

can be achieved by fixing the defects and faults found during the test.

REFERENCES

[1]. Mørk G, Barstow S, Kabuth A, Pontes MT. "Assessing the global wave energy potential," *ASME 2010 29th International conference on ocean, offshore and arctic engineering* 2010 Jan 1 (pp. 447-454). American Society of Mechanical Engineers.

[2]. Nejat P, Jomehzadeh F, Taheri MM, Gohari M, Majid MZ. "A global review of energy consumption, CO2 emissions and policy in the residential sector (with an overview of the top ten CO2 emitting countries)," *Renewable and sustainable energy reviews*. 2015 Mar 1;43:843-62.

[3]. Pelc R, Fujita RM. "Renewable energy from the ocean," *Marine Policy*. 2002 Nov 1;26(6):471-9.

[4]. Budar K, Falnes J. "A resonant point absorber of ocean-wave power," *Nature*. 1975 Aug;256(5517):478.

[5]. Evans DV. "A theory for wave-power absorption by oscillating bodies," *Journal of Fluid Mechanics*. 1976 Sep;77(1):1-25.

[6]. Mei CC. "Power extraction from water waves," *Journal of Ship Research*. 1976 Jun;20:63-6.

[7]. Antonio FD. "Wave energy utilization: A review of the technologies," *Renewable and sustainable energy reviews*. 2010 Apr 1;14(3):899-918.

[8]. French MJ, Bracewell R. "Heaving point absorbers reacting against an internal mass," *In Hydrodynamics of Ocean Wave-Energy Utilization* 1986 (pp. 247-255). Springer, Berlin, Heidelberg.

[9]. Bjarte-Larsson T, Falnes J. "Laboratory experiment on heaving body with hydraulic power take-off and latching control," *Ocean Engineering*. 2006 May 1;33(7):847-77.

[10]. Babarit A, Guglielmi M, Clément AH. "Declutching control of a wave energy converter," *Ocean Engineering*. 2009 Sep 1;36(12-13):1015-24.

[11]. António FD. "Phase control through load control of oscillating-body wave energy converters with hydraulic PTO system," *Ocean Engineering*. 2008 Mar 1;35(3-4):358-66.

[12]. Falnes J. "Wave-energy conversion through relative motion between two single-mode oscillating bodies," *Journal of Offshore Mechanics and Arctic Engineering*. 1999 Feb 1;121(1):32-8.

[13]. Beatty SJ, Buckham BJ, Wild P. "Frequency response tuning for a two-body heaving wave energy converter," *The Eighteenth International Offshore and Polar Engineering Conference*. 2008 Jan 1.

[14]. Korde UA. "Systems of reactively loaded coupled oscillating bodies in wave energy conversion," *Applied ocean research*. 2003 Apr 1;25(2):79-91.

[15]. Liang C, Zuo L. "On the dynamics and design of a two-body wave energy converter," *Renewable Energy*. 2017 Feb 1;101:265-74.

[16]. Cândido JJ, Justino PA. "Modelling, control and pontryagin maximum principle for a two-body wave energy device," *Renewable Energy*. 2011 May 1;36(5):1545-57.

[17]. Yu YH, Li Y. "Reynolds-Averaged Navier–Stokes simulation of the heave performance of a two-body floating-point absorber wave energy system," *Computers & Fluids*. 2013 Mar 15;73:104-14.

[18]. Al Shami E, Wang X, Zhang R, Zuo L. "A parameter study and optimization of two body wave energy converters," *Renewable energy*. 2019 Feb 1;131:1-3.

[19]. Nielsen, K., and P. F. Smed. "Point absorber—optimization and survival testing." *Proceedings of 3rd European Wave Energy Conference*. 1998.

[20]. Hirohisa, T. "Sea trial of a heaving buoy wave power absorber." *Proceedings of 2nd international symposium on wave energy utilization, Trondheim, Norway*. 1982.

[21]. Weber, J., F. Mouwen, A. Parish, and D. Robertson. "Wavebob—research & development network and tools in the context of systems engineering." *Proceedings of. Eighth European Wave and Tidal Energy Conference, Uppsala, Sweden*. 2009.

[22]. Li X, Chen CA, Xiong Q, Parker R, Zuo L. Design and Simulation of a Novel Mechanical Power Take-Off for a Two-Body Wave Energy Point Absorber. InASME 2018 International Design Engineering Technical Conferences and Computers and Information in Engineering Conference 2018 Aug 26. American Society of Mechanical Engineers.

[23]. Li Z, Zuo L, Luhrs G, Lin L, Qin YX. Electromagnetic energy-harvesting shock absorbers: design, modeling, and road tests. IEEE Transactions on Vehicular Technology. 2013 Mar;62(3):1065-74.

[24]. Cummins WE. The impulse response function and ship motions. David Taylor Model Basin Washington DC; 1962 Oct.

[25]. Lee CH. WAMIT theory manual. Massachusetts Institute of Technology, Department of Ocean Engineering; 1995.

[26]. Lawson M, Yu YH, Nelessen A, Ruehl K, Michelen C. Implementing nonlinear buoyancy and excitation forces in the WEC-Sim wave energy converter modeling tool. InASME 2014 33rd International Conference on Ocean, Offshore and Arctic Engineering 2014 Jun 8. American Society of Mechanical Engineers.

[27]. Qualisys AB. Qualisys motion capture systems. URL: http://www. qualisys. se/, accessed on. 2008:04-.

[28]. Gunawan B. WAVE ENERGY PRIZE TESTING AND DATA ANALYSIS OVERVIEW. Sandia National Lab.(SNL-NM), Albuquerque, NM (United States); 2018 Feb 1.

[29]. Payne G. Guidance for the experimental tank testing of wave energy converters. SuperGen Marine. 2008 Mar.

[30]. Falnes J. Ocean waves and oscillating systems: linear interactions including wave-energy extraction. Cambridge university press; 2002 Mar 21.